

Article

Battery Degradation Minimization-Oriented Hybrid Energy Storage System for Electric Vehicles

Cong Zhang ¹, Dai Wang ^{1,2,*}, Bin Wang ¹ and Fan Tong ¹

¹ Lawrence Berkeley National Laboratory, Berkeley, CA 94720, USA; congzhang@lbl.gov (C.Z.); wangbin@lbl.gov (B.W.); FanTong@lbl.gov (F.T.)

² Tesla Inc., 3500 Deer Creek Rd, Palo Alto, CA 94304, USA

* Correspondence: daiwang@tesla.com

Received: 4 November 2019; Accepted: 2 January 2020; Published: 3 January 2020



Abstract: A battery/supercapacitor hybrid energy storage system is developed to mitigate the battery degradation for electric vehicles. By coordinating the battery and supercapacitor, the proposed system avoids using the large bidirectional DC/DC. Through the improved topology and two added controlled switches, the battery current can be managed flexibly. Based on the battery and supercapacitor voltage, seven operation modes of battery and capacitor cooperation are designed. The control strategy is redesigned to match the modes, in which the key control parameters are calibrated based on three standard driving cycles. During driving, the proposed system calls the predefined parameter set by the cycle recognition technique. The objective of the cycle-related control is to maximize the harvest of the braking energy and minimize battery degradation in various driving styles. Taking the battery case solely as a benchmark and the infinite supercapacitors case as the largest battery degradation mitigation scenario, the battery degradation quantification of the proposed energy storage system shows more than 80% mitigation of the maximum theoretical battery degradation mitigation on urban dynamometer driving schedule (UDDS), highway fuel economy cycle (HWFET), and high-speed (US06) driving cycle, respectively. During the tested driving cycles, the simulation result indicates the battery degradation reduced by 30% more than the battery solely scenario, which proves the benefit of the proposed system.

Keywords: electric vehicles; hybrid energy storage system; supercapacitor; battery life; electric vehicles

1. Introduction

Both greenhouse gas (GHG) emission and fossil fuel consumption have been critical environment topics in recent decades. Compared to the conventional vehicle, the electric vehicle (EV) has advantages in energy consumption, exhaust emission, and average maintenance cost [1]. The lithium-ion battery is used as the supply source widely for electric vehicles [2], including the plug-in hybrid electric vehicles (PHEV) [3], battery electric vehicles (BEV), and fuel cell electric vehicles (FCEV) [4]. However, there are two concerns in the lithium battery application, including the expensive energy capacity and the limited driving environment, which limits the promotion of electric cars. Mitigating the battery capacity degradation and prolonging the battery life are two key goals in the battery energy management system [5].

During the vehicle configuration, the energy storage system is required to meet both the power and energy demand. For the lithium-ion battery, the power density is relatively lower than energy density. However, the capacitor is just the opposite. In the energy storage system (ESS) configuration, the charging mileage requirement should be met firstly [6]. Considering the power density features, the power configuration is not high enough. As a result, the battery suffers high discharging current, which accelerates the capacity degradation rate; that is to say, the strong discharge current accelerates

the degradation [7]. Furthermore, frequent charging and discharging are harmful to battery life [8,9]. In some extreme driving situations, the battery may be overcharged and discharged, which reduces the battery lifecycle seriously [10,11]. To solve the problem, the supercapacitor (SC) is usually configured to assist the peak power demand [12]. Moreover, increasing the battery size is another method to enhance the power demand of ESS. However, this method leads to high configuration costs. Further, with the battery size raising, the balancing difficulty among battery cells increases exponentially [13]. Using the SC can avoid the above issues in the ESS design. Also, in terms of maximizing energy efficiency, it is crucial to make good use of the harvested braking energy. As the power source, the SC can supply higher power. Adding the supercapacitor to the energy storage system, the frequent discharging and charging flow across the battery can be avoided [14,15]. The literature describes the advantages of the hybrid energy storage system (HESS) [16]. First, the supercapacitor can be used to protect the lithium-ion battery from the peak-power discharging. Secondly, because the SC has a higher energy efficiency than that of battery, including the SC can improve efficiency and reduce energy loss. Thirdly, the supercapacitor can work in a wider temperature range. Finally, since the supercapacitor can absorb the braking energy, the equipped battery can skip the frequent charging operations during braking situations [17].

For the purpose of improving the above issues, multi-new hybrid energy storage system has been proposed [18–32], including the novel HESS topology and the control strategy. In the previous proposed HESS topologies, there were three main types [18]: Passive, semi-active, and fully active, which will be introduced in the following section. The passive topology is simple, there are no requirements for control or expensive power electronic converters. However, during the power source working process, the voltage of SC is same as the voltage of battery. Therefore, the SC cannot charge/discharge at peak power rate. The major problem with this topology is that it cannot effectively utilize the UC stored energy [19]. In contrast, the fully active topology is the most complicated, which adopts two bi-directional DC/DC converters [20]. It has a good effect but the most expensive cost. As for the semi-active topology, it can provide a good trade-off between the passive topology and fully topologies. At present, the semi-active topology is the HESS research hotspot. In order to minimize the cost of HESS, Jose et al. came up with an interleaved controlled bidirectional converter topology to reduce the size of traditional DC/DC converter and extend the battery lifespan [21]. Ziyong et al. adopted the unidirectional DC/DC converter to optimal the system cost and quantify battery capacity loss by adding an additional diode. In this improved case, the unidirectional DC/DC converter size can be configured to a smaller size [14]. Odeim et al. studied the energy management algorithm with the genetic strategy and investigated the power load between the battery and supercapacitor with the optimization of multi-objective [22]. Cao et al. used a new HESS topology to optimize the system cost, however, the efficiency of braking energy regenerating is not high [20]. Song et al. researched the temperature and battery influence on the optimized HESS; the simulation shows that the HESS configuration and energy management system is robust to the temperature variations and battery price [23]. According to the state of charge (SOC) of the supercapacitor, the core point is to set the changeable battery discharge power limitation in their method. Because of the HESS topology, to configure a large DC/DC converter is unavoidable [24]. According to the previous literature, the full functioning of battery/SC topology and the DC/DC cost are expensive and complicated [14,20]. For example, the bi-directional DC/DC converter has a better function, but it is more expensive than the unidirectional type [25].

Besides the HESS topology, another important issue in HESS is the control strategy. The purpose of the control strategy is to regulate the best power flows sharing to prolong the battery lifetime. There are two control routes depicted in the literature [26], rule-based approach [27] and optimization-based approach [28,29]. In order to improve the regenerative braking energy, Naseri et al. improved an improved regenerative braking system. The PI controller is used to adjust the braking torque by regulating the duty-cycle of the PWM algorithm. The features of the improved regenerative braking system can achieve constant torque regenerative braking for realizing comfort and security

purposes [30]. Maciej et al. used the genetic algorithm strategy to optimize the fully active HESS system to decrease the battery degradation and extend the battery lifespan. Since the minimum number of DC/DC converters is two in the HESS, the whole system cost is still high [31]. Nassim et al. researched the new control strategy of HESS by reducing the battery power current to reduce battery decay. Santucci et al. have proposed to organize the energy management of a three sources hybrid electric vehicle in two-level. The first level was managed by an optimization-based control strategy while the second level can be managed by a rule-based or an optimization-based EMS [32]. Wang et al. have proposed a real-time optimization-based control strategy for a battery–SCs HESS using a single DC/DC converter. Validation on a standard urban driving cycle ECE-15 considered known in advance has been performed [33]. Whatever the approach for the HESS control, the variations of the driving cycle affect the HESS performances. Indeed, the HESS parameters are usually determined for a specific driving cycle that represents an ideal case.

Since the energy density of lithium-ion is much larger than the supercapacitor, the battery is usually regarded as the primary energy source in HESS [12]. Furthermore, the coordination between battery and SC should guarantee that the HESS can harvest the regenerative braking energy at high efficiency. Figure 1 is a brief overview of the traditional HESS topologies.

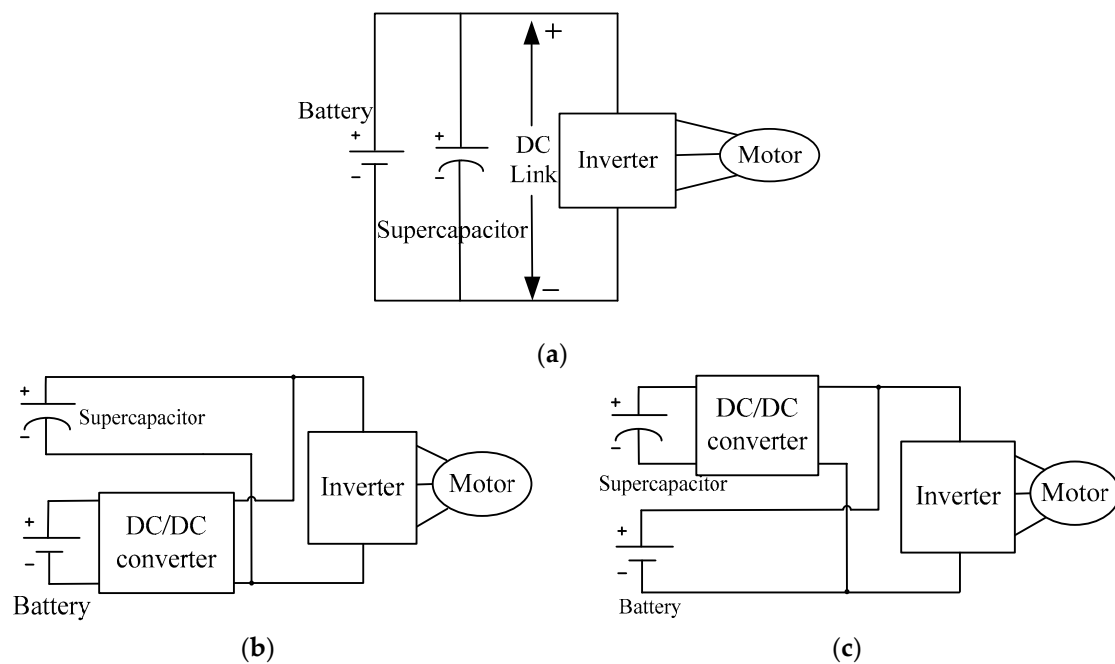


Figure 1. Different hybrid energy storage system (HESS) topologies: (a) passive parallel topology; (b) battery/supercapacitor (SC) configuration; (c) SC/battery configuration.

1.1. Passive Parallel Topology

Figure 1a shows the typical parallel topology of the HESS. Since the battery voltage range is narrow compared with SC voltage, the SC cannot make good use of its wide voltage range. Generally, the typical end of discharge battery voltage is around 80% of the nominal battery voltage ($V_{nominal}$) [34], i.e., the usable battery voltage is $[0.8V_{nominal}, V_{nominal}]$. In this topology, the SC voltage is also constrained by the same voltage range as the battery. The SOC of SC is calculated as follows:

$$E_{sc} = \frac{1}{2}CV^2, \quad (1)$$

$$SOC_{sc} = \frac{\frac{1}{2}CV^2}{\frac{1}{2}CV_{max}^2} = \frac{V^2}{V_{max}^2}. \quad (2)$$

E_{sc} is the stored energy in the supercapacitor, the unit is J. C is the capacitance of supercapacitor, the unit is F . V is the supercapacitor voltage, V_{max} is the maximum voltage of supercapacitor. SOC_{sc} is the supercapacitor state of charge. According to the above equations, about 64% of the total energy stored in SC cannot be discharged. Equally, in order to realize the same usable energy in SC, the SC size requirement will be higher in the basic passive parallel topology than other topologies that use DC/DC converter. In this topology, the advantage is the low-cost configuration. No DC/DC converter is needed in the passive parallel topology. In contrast, the disadvantage is the low utility percentage of the total stored energy in SC is the main disadvantage. The voltage of SC has to follow the battery voltage, which limits the use of large power density characteristics of the SC.

1.2. Battery/SC Topology

Figure 1b indicates the battery/SC topology. In this topology, the DC/DC converter connects the battery and SC. Because of the bidirectional DC/DC converter, the working voltage range of SC is much wider than that in basic passive topology. The advantage of this topology is that a wider SC voltage range is conducive to the potential charging/discharging capacity of the SC. Because of higher coulombic efficiency, this topology is helpful to improve energy efficiency when harvesting the regenerative braking energy. The disadvantage of this topology is that the SC does not have enough usable energy stored. Besides, the DC/DC converter has to be set large enough to supply higher power from the battery to the motor, which increases the system cost.

1.3. SC/Battery Topology

Figure 1c shows the SC/battery topology diagram. Compared with the above topology, the difference is that the SC and the battery exchange the position with each other. The advantage of this topology is that the energy flow can avoid the DC/DC converter during the majority operation when the vehicle is driving. The energy loss of the DC/DC converter is lower than other topologies. In this topology, there are four disadvantages [14,15]: (a) The DC/DC converter leads to energy loss when current flows across converter [14]; (b) the frequent charging actions reduce battery life [35]; (c) the DC/DC converter needs to be configured at a large size [20]; (d) The battery energy of harvesting regenerative braking energy is lower than the SC [19].

1.4. Fully Active Topology

Figure 2a represents the fully active topology in which two bidirectional DC/DC converters exist [20]. In this topology, the SC, battery, and inverter are isolated separately, and the available voltage of SC can get the largest range. This topology makes good use of SC and assists the battery in the largest potential. They are all the advantages of this topology. In contrast, the dominated drawback of the topology is the high cost of two bidirectional DC/DC converters.

1.5. Multi-Input Topology

Figure 2b shows the multi-inputs topology, in which a multi-input bidirectional DC/DC converter works equally as the two bidirectional DC/DC converters [36]. This topology has the same features as the above fully active topology. The voltage range among SC, battery, and inverter are isolated absolutely. SC can reach a wider voltage range. The main disadvantages of the multi-input topology are the complicated structure and high cost of DC/DC converter configuration. Its pros/cons are similar to the fully active topology.

1.6. Semi-Active Topology (Bidirectional DC/DC Converter)

For the purpose of reducing the DC/DC converter size, Cao et al. came up with a new topology to leverage the full functionality of battery and SC, which is introduced in Figure 2c [20]. In this topology, a controlled switch is added to control the current flow direction. There is no controller component

between the SC and motor load when the SC voltage is too low to transfer the energy to motor load, the battery needs to supply the energy to both the motor load and SC even at high power demand. The advantage of this topology is the battery not only works as the unique power source during the low-power cases but also assists to supply power at high-power cases. The drawback focuses on the DC/DC converter. Since the bidirectional DC/DC converter is mandatory during the energy flowing between the motor load and battery, the efficiency of harvesting braking energy is not high when the SC is charged fully.

1.7. Semi-Active Topology (Unidirectional DC/DC Converter)

Figure 2d shows a lower-cost topology in which the above bidirectional DC/DC converter is replaced by the unidirectional DC/DC converter, which is proposed by Song et al. [14]. In this topology, five modes are controlled to realize the coordination between battery and SC for all possible situations. The novelty of this topology is the unidirectional DC/DC converter, rather than a bidirectional DC/DC converter. The unidirectional DC/DC converter can transfer the energy from the regenerative braking system to the battery when SC is fully charged. The advantage of this topology is that the unidirectional DC/DC converter has a lower cost than the bidirectional DC/DC converter. The drawback is that the charging efficiency is not high enough because of the energy consumption of the DC/DC converter. This topology cannot realize the high efficiency in both charging and discharge for the battery. Furthermore, the SC voltage is controlled strictly higher than the battery, which constrains the usable energy stored in SC.

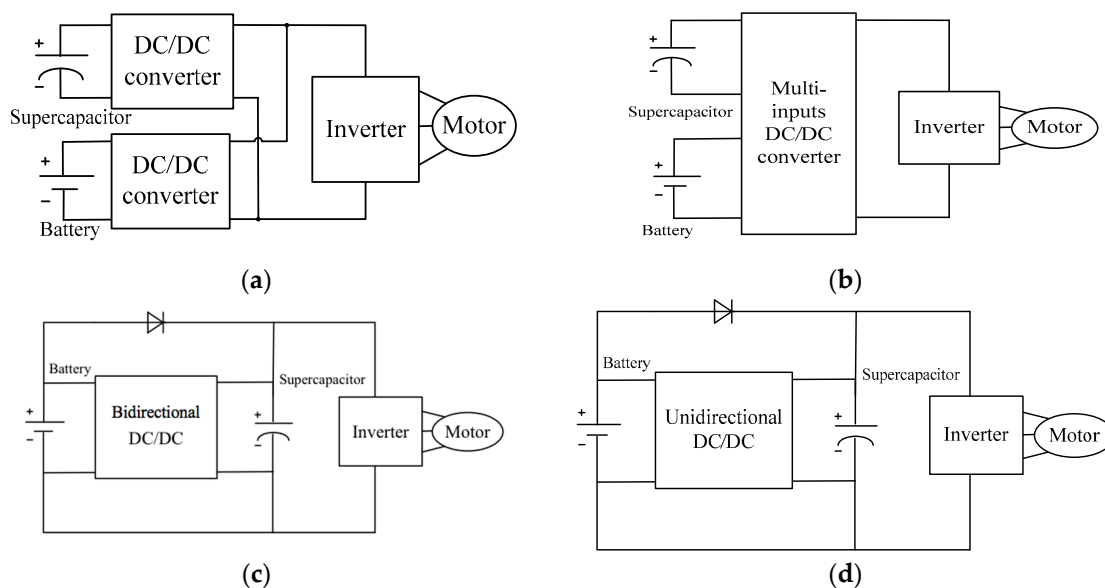


Figure 2. Different HESS topologies: (a) Fully active configuration; (b) multiple inputs DC/DC; (c) semi-active configuration incorporated (bidirectional); (d) semi-active configuration incorporated with a diode (unidirectional).

Although these prior studies are relevant for the research questions addressed in the present study, there are several limitations of the prior studies that justify the need and broad impact of the present study. Also, we proposed our contribution to this paper. Including:

1. Failed to develop the HESS topology and the changeable control strategy [14]. In this paper, the control strategy is developed based on the customized hardware topology.
2. To cover the high efficiency regenerative braking energy harvesting and the battery discharging, the previous literature failed to use the unidirectional DC/DC converter in the HESS topology [20]. In this paper, we improved the HESS topology by using the unidirectional DC/DC converter, with two switches.

3. Failed to improve the rule-based control strategy according to the driving cycles. In this research, the control threshold can be customized to mitigate battery degradation at various driving cycles [14,15].

4. Failed to investigate the combination among the HESS size configuration, topology, and the control strategy. In our research, we integrated them together, and presented the quantitative battery degradation is given across different scenarios.

This paper is organized as follows. Section 2 stresses the topology structure of the proposed HESS and describes the working modes in both driving conditions and braking conditions. The strategy is presented in Section 3. It is a rule-based control strategy, which matches the proposed HESS closely. In Section 4, we explain the battery degradation model, which is chosen as the objective function of searching for the key parameters of the control strategy. Simulation results are shown in Section 5. Conclusions and future work are in Section 6.

2. The Topology of the HESS

For the purpose of improving the current topology, this study proposes a new semi-active HESS topology (Figure 3). Besides inheriting the advantages in other semi-active topologies, the proposed topology also improves both the discharging and charging efficiency. During the HESS operation, there are seven modes in total. All operation situations can be identified as one of seven driving modes. It covers three modes in driving condition and three modes in braking condition.

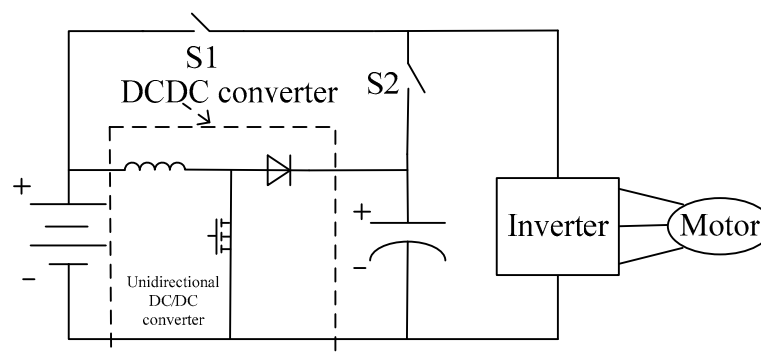


Figure 3. Proposed HESS topology.

2.1. Driving Condition

The driving condition is the most frequent action for vehicles. During the driving conditions, 4 modes of HESS are divided. When selecting each individual mode, the control strategy and topology deactivate or activate the switches' status by analyzing the power demand, battery, and SC SOC.

2.1.1. Mode 1: The Supercapacitor Working as the Unique Energy Source

When the SOC_{SC} is high enough ($SOC_{SC} \geq K0$), the SC supplies all required power solely. The precondition of this mode is the SC stores enough energy. The regenerative braking energy can charge SC to a high voltage ($SOC_{SC} \geq K0$). The SOC_{SC} is equal to the ratio between the voltage square and the maximum voltage square. In mode 1, the controlled switch S2 is connected (Figure 4).

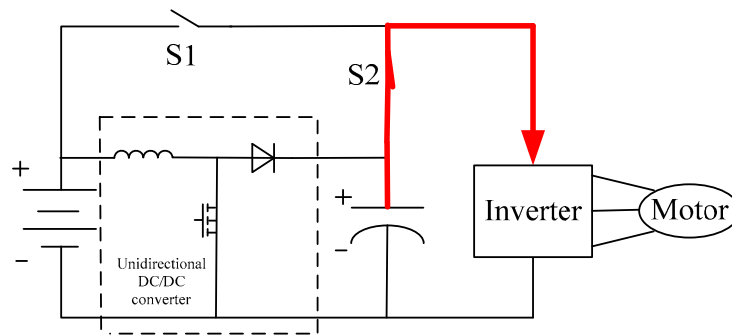


Figure 4. Mode 1—the SC acts as the unique power source.

2.1.2. Mode 2: The SC and Battery Supply Energy to Motor Load Together

In mode 2, the supercapacitor assists the battery to reduce the discharging power. When the SOC_{SC} is in the range $[K2, K0]$ and the power demand is larger than the power threshold ($P_{Threshold}$), both the battery and supercapacitor work as the energy source. The power distribution strategy will be shown in the next section. Here, the controlled switch S2 is connected (Figure 5).

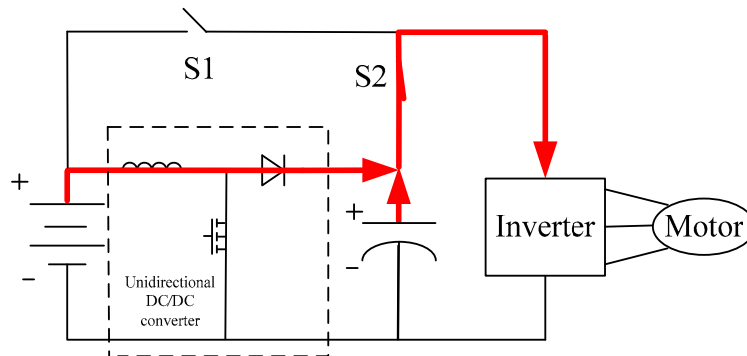


Figure 5. Mode 2—both the battery and supercapacitor discharge.

2.1.3. Mode 3: The Battery Acts as the Unique Power Source

In this mode, only battery charges the motor. There is no current flow between the battery and the SC. In this mode, there is no energy loss on the DC/DC converter. This mode can be triggered when one of the following two conditions is met: (a) The SC does not have enough energy stored; (b) the SC has sufficient energy stored, and the vehicle demanded power is lower than the $P_{threshold}$. Here, the controlled switch S1 is connected (Figure 6).

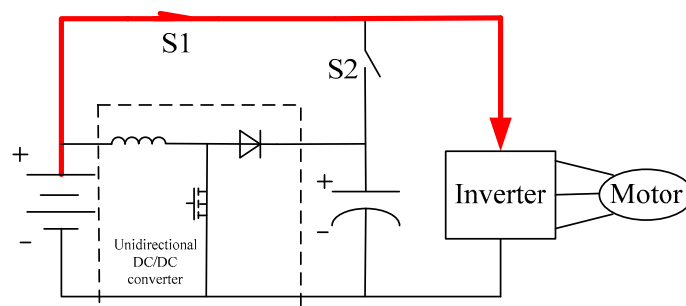


Figure 6. Mode 3—the battery acts as a unique power source.

2.1.4. Mode 4: The Battery Supplies Power to the Motor Load and SC Simultaneously

In mode 4, the lithium battery supplies energy to both the motor load and SC simultaneously. This mode can be activated when the conditions are satisfied at the same time: (a) The vehicle demanded

power is lower than $P_{threshold}$; (b) SOC_{SC} is lower than $K2$. Here, the controlled switch S1 is connected (Figure 7).

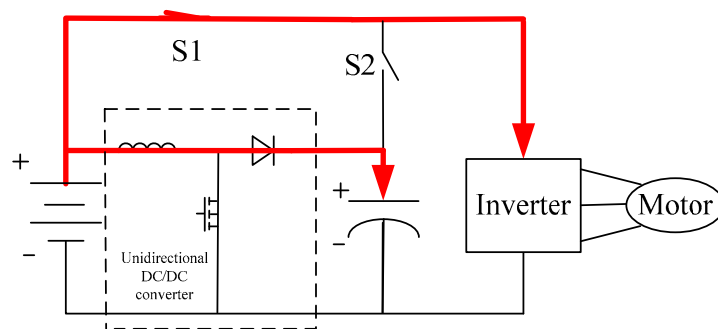


Figure 7. Mode 4—the battery supplies power to the motor load and SC simultaneously.

2.2. Braking Condition

There are two main controlled targets in the braking condition. Firstly, the braking energy should be harvested as much as possible; secondly, in order to protect the battery, the battery should avoid being charged frequently in braking conditions.

2.2.1. Mode 5: Both the Braking Energy and Battery Charges the SC

In this mode, all regenerative braking energy flows into the SC. In the meantime, the battery also charges the SC. This mode can be activated when the condition is satisfied: The SOC_{SC} is lower than $K1$, which aims to resume the SC energy as much as possible. Here, the controlled switch S2 is connected (Figure 8).

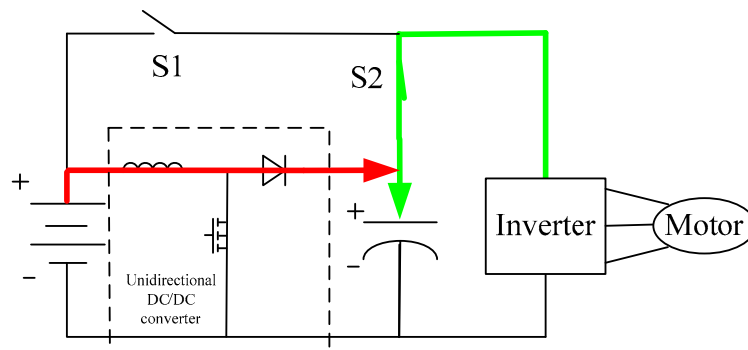


Figure 8. Mode 5—both the braking energy and battery charge the SC.

2.2.2. Mode 6: The SC Harvests the Braking Energy Solely

Compared with mode 5, the SC absorbs the energy from the regenerative braking system solely in mode 6. It is the most common mode during the braking process. Here, the controlled switch S2 is connected (Figure 9).

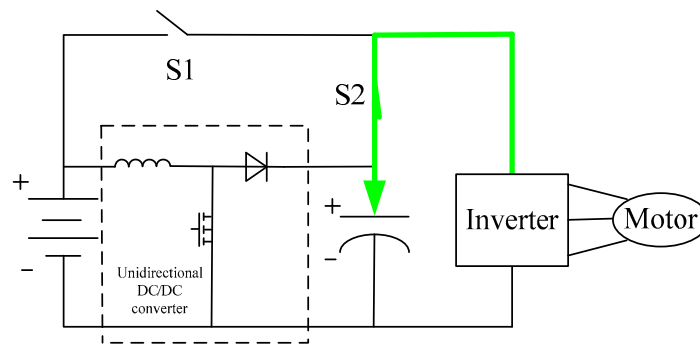


Figure 9. Mode 6—the SC harvests the braking energy solely.

2.2.3. Mode 7: The Battery Harvests the Braking Energy Solely

After the SC is charged to full ($SOC_{SC} \geq K0$) by regenerative braking energy, the SC has no available space to store the extra braking energy. The HESS controls the switch S2 to be disconnected and switch S1 to be connected. In this mode, the battery begins to harvest the regenerative braking energy. In other previous literature, either the battery or the SC acts as the only power source, which will harvest the braking energy. However, they cannot realize the balance between battery protection and redundant braking energy utility. Mode 7 is the action following mode 6 (Figure 10). There is an extreme situation when the battery driving downhill at a long distance. Because of the regenerative braking, the battery can be fully charged. In this situation, both S1 and S2 are disconnected.

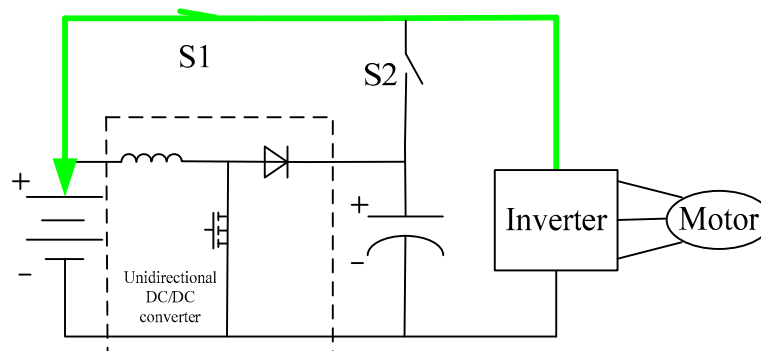


Figure 10. Mode 7—the battery harvests the braking energy solely.

Across the above seven modes, the switches S1 and S2 are the key components to control the current flow direction and route. In summary, the switch S1 is the connection between the battery and the motor. Once the energy flow transfer between the battery and motor, S1 will be connected. In contrast, switch S2 is the connection between the supercapacitor and motor. Once the energy flow transfer between the battery and motor, S2 will be connected.

$K0$, $K1$ and $K2$ are the SOC_{SC} thresholds— $P_{threshold}$ ($0.25 \leq K2 \leq K1 \leq K0 \leq 1$). $K0$ is the threshold above which the SC is regarded as fully charged; $K1$ is the SOC threshold above which the SC stops accepting the current from the battery. $K2$ is the SOC threshold under which the SC is not allowable to discharge. During the range $[K2, K1)$ of SOC_{SC} , $P_{threshold}$ is the demarcation point, which decides whether the battery charges the SC or not. In the meantime, $P_{threshold}$ also decides when the SC begins to assist the battery. The switch S1 is the connection between the battery and the motor. Once the energy flow transfers between the battery and motor, S1 will be connected. In contrast, switch S2 is the connection between the supercapacitor and motor. Once the energy flow transfers between the battery and motor, S2 will be connected. The type of controlled switch is IRGP4067DPBF [37].

2.3. Vehicle Model Specification

As to the demanded power calculation, this paper calculates the demanded power as follows:

$$\text{power demand} : P_{demand} = [ma + f(v) + mg \sin \theta] \times v \quad (3)$$

$$\text{Coast down curve} : f(v) = A + B \times v + c \times v^2 \quad (4)$$

where m is the vehicle weight, unit: kg. a is the acceleration of vehicle, unit: m/s^2 . v is the vehicle speed, m/s . g is the gravitational acceleration, equal to 9.8 m/s^2 . $f(v)$ is the coast down curve for the vehicle, including the rolling resistance and the aerodynamic resistance. $f(v)$ is the empirical resistance equation for a vehicle, which contains the aerodynamic drag and the rolling resistance [38]. A , B and C are the fitted parameters of the coast down curve. A : Unit is N, B : Unit is $\text{N}\cdot\text{s}/\text{m}$, C : Unit is $\text{N}\cdot\text{s}^2/\text{m}^2$. Coast down is one of the most frequent tests for vehicles and consists of vehicle launch from a certain speed with the engine ungeared, simultaneously recording the speed and traveled distance until the vehicle stops. This can be done for different reasons, mainly targeted to obtain valuable information about the general condition of the vehicle and about its interaction with the environment.

The battery and supercapacitor specification is introduced in [15]. Table 1 shows the basic unit parameters for both the supercapacitor and lithium battery.

Table 1. Unit parameters.

Specification	Supercapacitor	Battery
Capacity of unit	2000 F	44 Ah
Maximum voltage (V)	2.7	3.6

Figure 11 shows the statistical daily driving distance features [19]. Around 80 percent of the driving distance samples have a lower daily trip than 82 km. Furthermore, 96.6 km can meet 85% of the overall driving trips. Both the daily driving distance distribution and cumulative features are demonstrated in Figure 11.

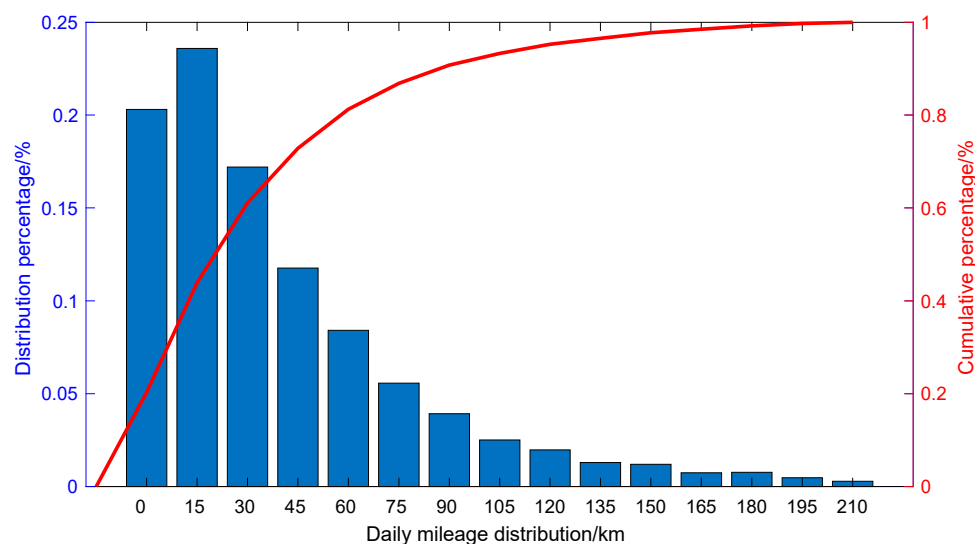


Figure 11. Daily driving features.

Taking the NISSAN Leaf as an example, the average measured energy consumption is $171.4 \text{ Wh}/\text{km}$ on the US06 cycle [19]. Aims to satisfy the majority (e.g., 85%) of the individual daily driving requirement (60 miles), even until the time when the battery needs to be replaced (supposing the battery retires after the remaining energy decreasing up to 70% of the primary capacity), the battery size should be

configured at least 23.66 kWh. Moreover, the temperature is an important factor that affects the HESS system. However, the temperature influence on the driving range is complicated. For a car with the same configuration, the vehicle's mileage is various across the different driving situation, including the temperature. In this paper, we calculate the energy requirement and configure the battery and SC size under the room temperature environment.

According to the previous studying, the supercapacitor units can be set as 76 [19]. The following is a brief introduction to the calculation process: First, the overall energy requirement for the power supply system is calculated by vehicle model and mileage requirement. Secondly, the extreme acceleration driving mode is used to calculate the energy requirement for SC. Thirdly, the energy requirement for the battery is obtained and divided by the battery cell parameters.

Therefore, the battery configuration should be set as follows:

$$E_{Bat} = E_{All} - E_{SC} \quad (5)$$

The battery units' number can be calculated as follows:

$$Number_{Bat} = \frac{E_{Bat}}{Energy_{Bat_cell}}. \quad (6)$$

E_{Bat} represents the configured battery package capacity. E_{All} represents the total energy requirement for the vehicle energy supply source. E_{SC} represents the configured supercapacitor package capacity. $Energy_{Bat_cell}$ is the rated capacity in Wh for each battery unit. Combining the feasible of configured HESS topology, the number of battery cells is chosen as 164. Since the battery package adopts the parallel structure of two cells, referring to Table 1, the battery package capacity is 88 Ah (equally, 1 C = 88 A).

For the motor, we adopt the same motor as the Nissan Leaf, and for the inverter, its specification is CSI 100-F2T, which support the 110–300 V voltage input [39].

The weight values of the components are described in Table 2.

Table 2. Component parameters.

Components	Model (kg)	Leaf (kg)
Base weight (kg)	1462	1462
Battery (kg)	146	181
DC/DC converter (kg)	10	N/A
Supercapacitor (kg)	27.4	N/A
Total weight (kg)	1645	1643
A	N/A	31.91
B	N/A	0.11159
C	N/A	0.017757

For Nissan leaf, the coast down curve is measured by the Argonne National Laboratory (ANL) [40]. Furthermore, they have the instantaneous power versus the time at different driving cycles. The above table shows that the mass between the leaf and models in the paper is similar. Based on leaf measured data, this study adopts Equation (7) to deduce the power demanded in the configured model.

$$E_{model} = \frac{Weight_{model}}{Weight_{Leaf}} \times E_{Leaf} \quad (7)$$

E_{model} represent the energy consumption of the configured, $Weight_{model}$ represents the total mass of the configured model, including the DC/DC converter, battery package, and DC/DC converter [41]. $Weight_{leaf}$ represents the total mass of Nissan Leaf. E_{Leaf} is the measured energy consumption for Nissan Leaf. Equation (7) shows that the fuel consumption rates between Leaf and HESS models are

approximately equal. Specifically, the leaf can represent the model fuel consumption on the typical driving cycles.

3. Evaluate the Battery Degradation

The main object of this research is to explore the SC influence on battery degradation. There are two kinds of battery degradation: Calendar degradation and cycle degradation. Calendar degradation results from time going, and it is not much different for different usage cases. In this paper, only the battery cycle loss is considered. From the above equations, the battery degradation loss can be concluded that the greater the battery discharge power, the faster the battery decaying. According to the previous literature, the battery cycle degradation rate is influenced by the cumulative integral of the circuit and instant discharging value [7]. In HESS, the lithium battery contributes the majority needed energy. However, the supercapacitors can help to decrease the battery degradation rate at the peak power demand period.

This paper quantifies the capacity degradation of lithium battery and compares the degradation values between the proposed HESS and the battery solely case. According to previous literature [36], the battery degradation exponential equation is used as follows:

$$D_{cycle} = (\alpha \times T^2 + \beta \times T + \gamma) \exp[(\delta \times T + \epsilon) \times I_{rate}] \times Ah_{Through} \quad (8)$$

$$D_{calendar} = \mu \times t^{0.5} \times \exp[-E_a / (R \times T)] \quad (9)$$

$$D_{all} = D_{cycle} + D_{calendar} \quad (10)$$

where $\alpha \times T^2 + \beta \times T + \gamma$ and μ are pre-exponential factors, T is the absolute temperature, $\alpha, \beta, \gamma, \delta, \epsilon$ are fitted parameters of the curve, I_{rate} is the current C rate, $Ah_{Through}$ represents the amount of charge delivered by the battery during cycling, T is the days, E_a is the activation energy in $\text{J} \cdot \text{mol}^{-1}$, and R is the gas constant. D_{cycle} , $D_{calendar}$, and D_{all} are the cycle battery degradation, calendar degradation, and total degradation, respectively. These parameter values are listed in [7].

Once the electric current is flowing between the SC and the battery, the total energy loss of HESS will increase. Approximately all energy flowing from SC can be regarded as the battery output. During the discharging process of HESS, the cumulative energy flowed from SC consumes $1 / (\eta_{DC/DC} \times \eta_{SC})$ times energy from the battery. Here, $\eta_{DC/DC}$ and η_{SC} are DC/DC converter efficiency and SC coulombic efficiency, respectively. In this research, the DC/DC converter efficiency is set as 95%, and the SC coulombic efficiency is set as 92% [42,43].

4. The Control Strategy of the HESS

The core part of the control strategy for HESS is the instantaneous control for SC voltage. This is different from the previous literature, in which the formulation is created based on the speed [35].

$$SOC_{exp} = 1 - \frac{\min(3 \times V_{vehicle}, 160)}{160} \quad (11)$$

$$V_{exp} = \sqrt{1 - \frac{\min(3 \times V_{vehicle}, 160)}{160}} \times V_{max} \quad (12)$$

SOC_{exp} represents the expected SOC of supercapacitor, $V_{vehicle}$ is the vehicle speed, V_{exp} is the SC voltage expectation value, and V_{max} represents the largest SC voltage. This strategy is easy to control the SC voltage, but there are some drawbacks.

In mild driving situations, the vehicle power demand is not high. For the purpose of making good use of battery energy, the battery can act as the unique power source to avoid energy loss in the DC/DC converter and SC. As for the aggressive driving situation, the power demand is much higher than the power demand in a mild driving cycle. In such cases, the SC needs to power the vehicle.

However, different drivers have different driving behaviors, so it is impossible to get a set of fixed control thresholds to meet all kinds of driving situations. Furthermore, the energy capacity of SC is limited, and it is impossible to assist the battery too much. The controller should have the ability to adjust the SOC of SC instantaneously. The previous control strategy is the global optimization to realize the overall optimization for the majority of driving situations, but it cannot realize the best control for every kind of driving cycle. This study comes up with a variable control algorithm to implements the HESS optimized control in different driving situations (UDDS, HWFET, and US06).

4.1. Control Strategy Diagram

This paper uses the decision-tree function to coordinate the power allocation between the supercapacitor and lithium battery (Figure 12). Based on the previous HESS topologies, some new improvements are added. Further, seven operation modes are divided into driving. When the SOC_{SC} is changing in the range from 0.25 to 1, the controller adopts different power allocation strategies between the battery and SC.

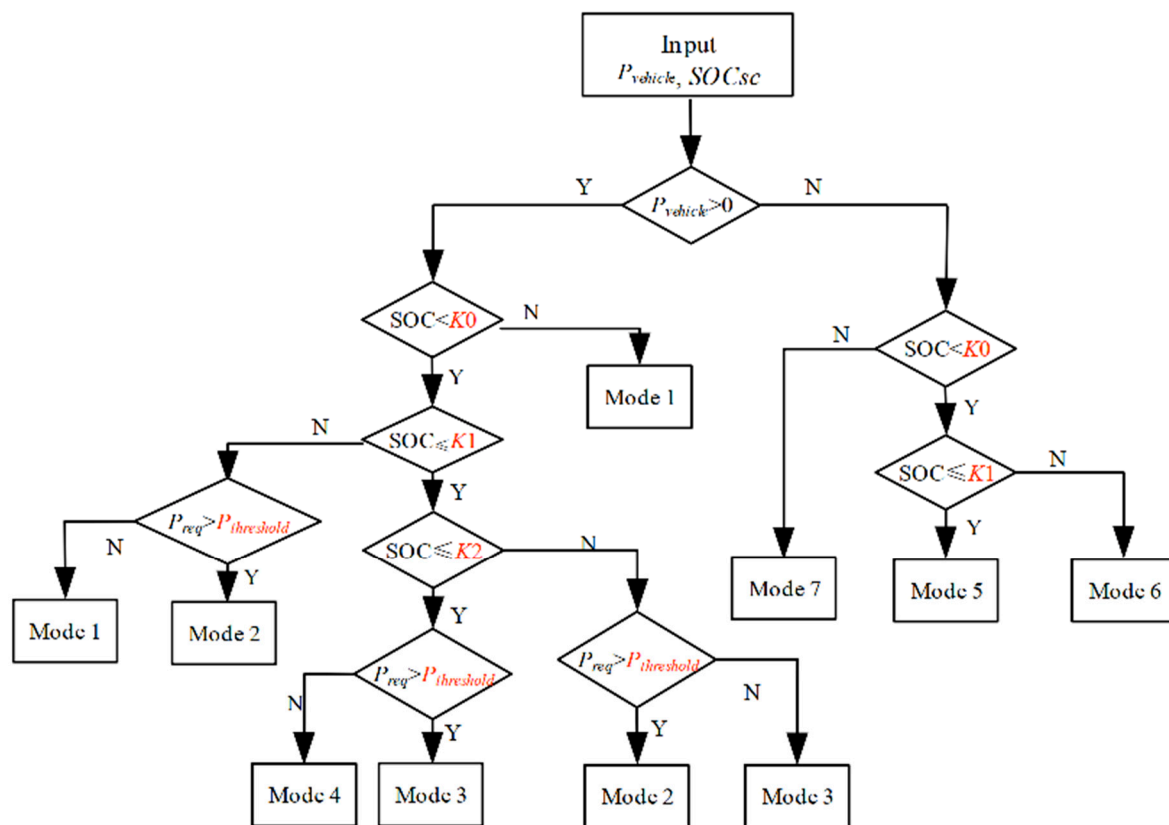


Figure 12. Rule-based algorithm.

Different from the chemical application in lithium battery, the supercapacitor keeps the energy by using the physical features. Theoretically, all stored energy in the SC can be discharged totally. Because of safety reasons, one-quarter of the maximum energy does not get used in the supercapacitor [44]. Based on Equations (1) and (2), the working voltage of SC is from $\frac{1}{2}V_{max}$ to V_{max} [21,44]. During the real-time control, the HESS chooses the exact working mode based on the demanded vehicle power and instantaneous SOC_{SC} . Under the initial situations, the switch S1 and S2 is disconnected. The strategy details are listed as follows:

Step 1, judge the driving or braking mode based on the driving action.

Step 2, if the vehicle is in the driving condition, mode 1–4 will be implemented. The SOC_{SC} , demanded power and power threshold decide which mode is activated. Including:

SOC_{SC} is in the range of $[K0, 1)$, which represents the SC is fully charged. In order to keep storage space for the regenerative braking, SC can supply all demanded vehicle power solely.

SOC_{SC} is in the range of $[K1, K0)$, which represents the SC owns sufficient energy. If the vehicle demanded power is larger than the threshold ($P_{threshold}$), both the battery and SC supply power together. Mode 2 will be activated. If the vehicle power demand is no larger than the threshold ($P_{threshold}$), mode 3 will be activated. In mode 3, only the battery supplies the energy. The switch S1 is connected.

SOC_{SC} is in the range of $[K2, K1)$, which represents the SC stays on the medium energy level. In this situation, if the demanded power is larger than the $P_{threshold}$, model 2 is activated. In this mode, the SC and the battery discharge the energy together. Once the demanded power is larger than $P_{threshold}$, mode 3 will be activated.

SOC_{SC} is in the range of $[0, K2)$, which represents the SC has insufficient energy. In this situation, if the demanded power is higher than $P_{threshold}$, the battery supplies the energy to motor solely (mode 3). Otherwise, the battery powers the motor load and charge the SC at the same time (mode 4). However, the maximum discharging power of the battery is no larger than $P_{threshold}$.

Step 3, when the vehicle drives in the situation of braking, modes 5–7 will be activated.

SOC_{SC} is in the range of $[K0, 1)$, which represents that the SC has sufficient energy. For the purpose of improving energy efficiency, the battery needs to harvest the regenerative braking energy (mode 7). The controller switch S1 is connected. However, in order to protect the battery, mode 7 does not appear frequently.

SOC_{SC} is in the range of $[K1, K0)$, which represents the SC stays on the medium energy level. In order words, the SC still has available space to harvest the regenerative braking energy (mode 6).

SOC_{SC} is in the range of $[0, K1)$, which represents the SC has insufficient energy. In preparation for the next peak power demand, the SC needs to be charged soon. Besides the regenerative braking energy charging the SC, the battery also charges the SC at constant power. Here, mode 5 is activated.

4.2. Determine the Key Thresholds of the Rule-Based Control Strategy

In the above control strategy, seven HESS operation modes are defined based on the HESS status. The factors which decide the mode selection, consist of the power demand, SC SOC. During the multi-comparison, there are four parameters are included: $K0$, $K1$, $K2$ and $P_{threshold}$. The values of the four parameters are different across different cycles. For a certain driving cycle, there is a group of parameters, which can realize the minimum battery current. This paper explores the optimized parameters configuration in the control algorithm, which matches the proposed HESS topology.

In the control strategy, there are four parameters ($K0$, $K1$, $K2$ and $P_{threshold}$) to be determined. $K0$ is the SOC_{SC} threshold above which the SC is regarded as sufficient energy stored (or fully charged). $K1$ is the SOC_{SC} threshold under which the SC will need the extra charging from the battery when the battery has spare discharging power space. $K2$ is the SOC_{SC} threshold under which the SC is regarded as insufficient energy stored and stops assisting HESS discharging. $P_{threshold}$ is the power threshold, which is used to judge whether the power demand is high or not. For example, if the demanded power is larger than $P_{threshold}$, the demanded power can be regarded as high-power demand. In this research, the control algorithm uses the automatic searching strategy to explore the optimized configuration for the above parameters, which is shown in the Algorithm 1. It is an itinerate loop to find the optimized parameters set for the thresholds. In the control strategy, 1CP means the discharging value of power at which all energy stored in the battery can be discharged out in an hour. For the 24 kWh battery package, $1CP = 24 \text{ kW}$ [19].

For $K0$, its constraint is

$$0.90 \leq K0 \leq SOC_{SC,max}. \quad (13)$$

For $K1$, its constraint is

$$0.5 \leq K1 \leq SOC_{SC,max}. \quad (14)$$

For K_2 , its constraint is [17,22]

$$SOC_{SC,min} \leq K_2 \leq 0.5. \quad (15)$$

For $P_{threshold}$, its constraint is

$$0 \leq P_{threshold} \leq 1CP. \quad (16)$$

Algorithm 1 Code structure of searching the parameter set.

```

for  $K_0 = 0.9: \Delta : SOC_{SC,max}$ 
for  $K_1 = 0.5: \Delta : SOC_{SC,max}$ 
for  $K_2 = SOC_{SC,min} : \Delta : 0.5$ 
for  $P_{threshold} = 0: \Delta SOC_{step} : 1CP$ 
    Calculate battery degradation
    Choose the smaller one after every iteration
result:  $K_0, K_1, K_2, P_{threshold}$ , which results in the smallest battery degradation.

```

5. Results

In theory, the battery can work at a constant discharging power if the SC size can be configured large enough [19]. Combined with the battery degradation feature, the battery can realize the minimum degradation when discharging at a constant value. The infinite SC case means that the SC is configured large enough and the SC can supply unlimited power. In reality, the infinite SC case cannot be realized because of the actual cost constraint. The battery degradation gap between infinite SC case and battery solely case represents the largest battery degradation mitigation. Taking the HWFET as an example, Figure 13 shows the battery current in these three different scenarios: Battery solely, optimized HESS, and infinite SC cases. For the optimized HESS case, the battery current can avoid the peak discharging periods effectively, such as the moment 300 s and 625 s. As for the infinite SC case, it represents the ideal scenario in which the battery works at the average power.

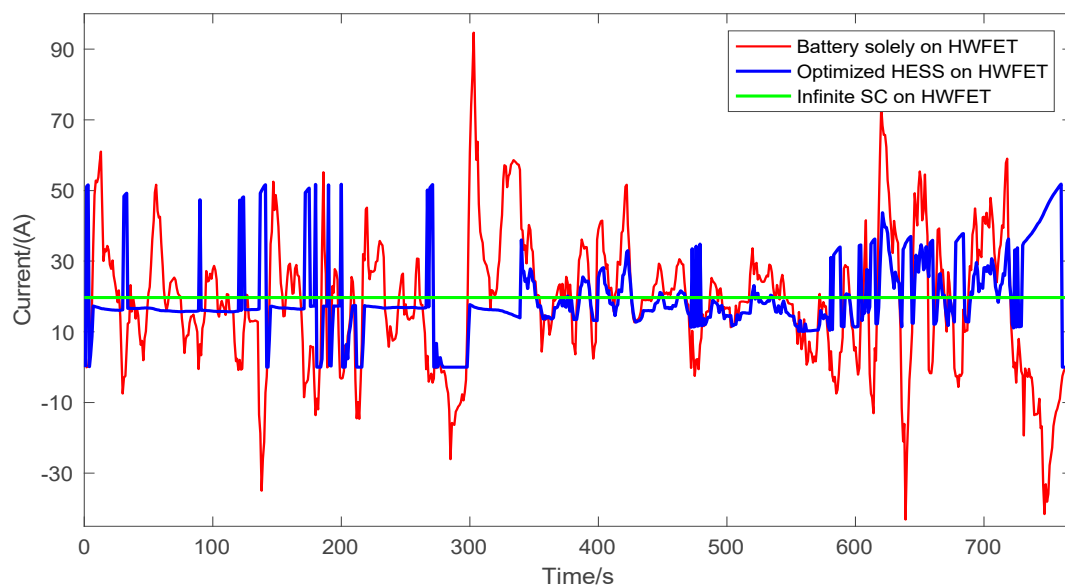


Figure 13. Battery current in different scenarios.

In order to quantify the battery current improvement in different range, Figure 14 shows the battery current fractions in each discharging/charging current range. The negative battery current shows the regenerative process of braking. Compared with the battery solely case, the optimized HESS reduces the battery charging frequency largely during braking. For example, all high regenerative braking current (higher than -0.25 C) is avoided. Instead, the braking energy charges the SC rather

than the battery. Similarly, the high battery discharging power period has also been shortened, such as the discharging current range 0.5–0.75 C and higher than 0.75 C. Overall, the optimized HESS moves the peaking discharging and charging current to the mild and small current range, e.g., range 0–0.25 C.

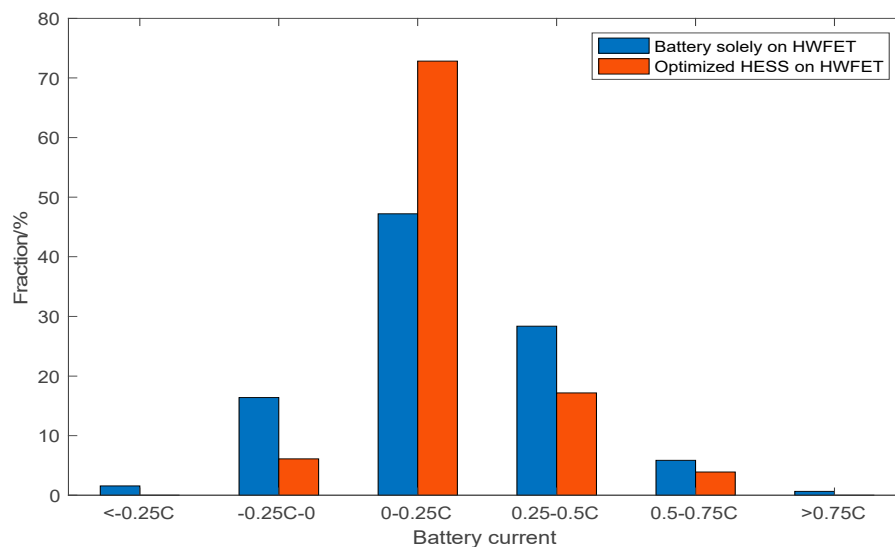


Figure 14. Battery current distribution.

In this research, a concept of realization percentage is used to evaluate the mitigation effect of the new proposed optimal HESS system.

$$\text{Realization percentage} = \frac{D_{\text{Optimal}} - D_{\text{Infinite}}}{D_{\text{Battery_solely}} - D_{\text{Infinite}}} \times 100\% \quad (17)$$

where D_{Optimal} is the battery degradation value in new proposed HESS system, D_{Infinite} is the battery degradation in infinite SC case, and $D_{\text{Battery_solely}}$ is the battery degradation in battery solely case. In theory, $D_{\text{Infinite}} \leq D_{\text{Optimal}} \leq D_{\text{Battery_solely}}$, the larger the *Realization percentage* is, the larger mitigation on battery degradation can be realized.

After launching the searching algorithm, four-parameter sets can be deduced for any specific driving cycle. Table 3 shows the battery cycle loss on these different tested cycles. According to the simulation, the HESS can get as high as 93.79%, 94.44%, and 82.72% of the theoretical mitigation potential of battery degradation on UDDS, HWFET, and US06, respectively.

Table 3. Searching results for parameters.

	UDDS	HWFET	US06
Test distance (km)	71.9	99.0	66.3
Average power (kW)	2.75	5.77	11.17
K0	0.96	0.94	0.98
K1	0.9	0.82	0.81
K2	0.25	0.25	0.25
$P_{\text{threshold}}$	3.12	6.24	13.92
Battery degradation (10^{-4})	On the tested driving cycles		
Infinite SC (%)	37.73	46.37	77.23
Optimal (%)	38.83	46.79	85.1
Battery solely (%)	55.43	53.92	122.78

Taking our own recorded driving cycle as an input to validate the developed control system, Figure 15 shows the speed profile of the trip. This trip is a combined trip, which contains both the city and highway driving features. Figure 16 shows the battery degradation comparison among different HESS. Table 4 gives the cumulative battery degradation values of all kinds of energy storage system. Among all scenarios, the battery size is the same, which is 23.66 kWh. Especially, the energy management algorithm is same for all topologies. Based on Figure 16 and Table 4, the following items can be concluded: (1) The infinite SC case represents the ideal control situation, in which the battery can discharge at the average constant current and realize the least battery degradation. It locates at the lowest position in cyan color. (2) In contrast, the battery solely case represents the worst case, in which the battery experiences the largest degradation. In this topology, there is no SC as an assisted power source. Generally, the previous two scenarios represent the best and worst battery degradation. (3) For the simple parallel structure as 1a (refer to Figure 1a), its benefit on mitigating battery degradation is very limited. The battery degradation is 11.62×10^{-4} , which is close to the battery solely case. It means the battery degradation mitigation is limited in this case. (4) “Refer 2c” case is the semi-active HESS with bidirectional DC/DC converter included, which represents a high configuration cost. Except for the unlimited SC case, “Refer 2c” is the HESS topology which has the best battery degradation mitigation. (5) In the proposed HESS, the battery degradation decreased from 11.90×10^{-4} to 8.33×10^{-4} (reduced by 30%), which is closed “Refer 2c” case. (6) “Refer 2a” case is the fully active HESS with two bidirectional DC/DC converter included. However, the energy loss of converters leads to the larger energy consumption of the battery. The battery degradation is close to the proposed HESS and refer 2c. (7) “Refer 1b” case is the battery/SC topology in which the bidirectional DC/DC converter included. Compared to the “Refer 2a”, the missing of diode leading to the overflow of the energy, which leads to energy loss and increases the battery degradation.

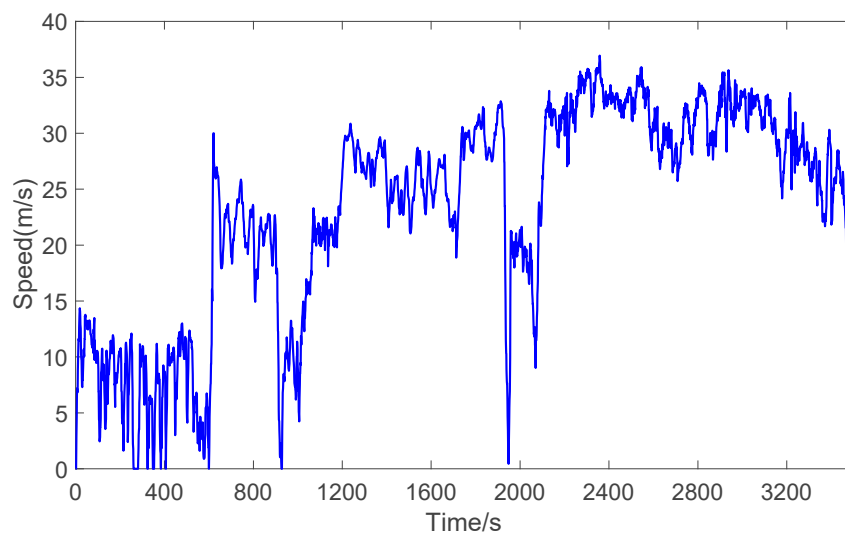


Figure 15. The combined driving cycle.

Table 4. The accumulative battery degradation on the tested driving cycle.

Types	Infinite SC	Battery Solely	Proposed HESS	Refer 1a	Refer 1b	Refer 2a	Refer 2c
Degradation (10^{-4})	7.48	11.90	8.33	11.62	10.12	8.77	8.08

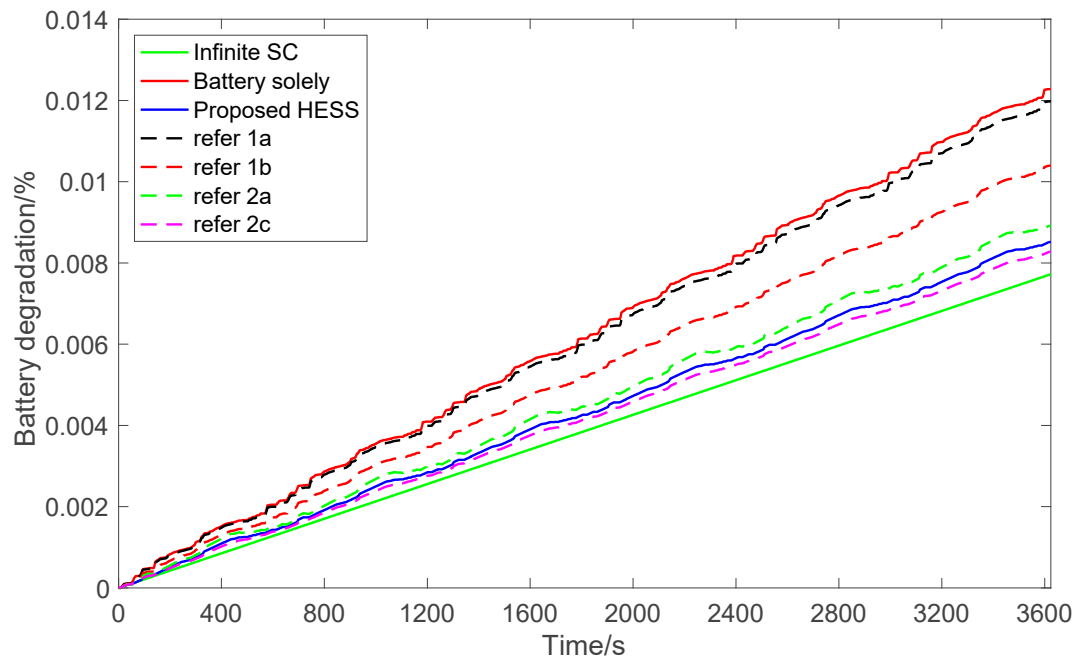


Figure 16. Battery degradation comparison in different HESS.

6. Conclusions

This paper proposes a new HESS system, which consists of a novel topology and a customized control algorithm. The improvements include reducing the DC/DC converter size, avoiding frequent discharging and charging to the battery, and maximizing braking energy regeneration. By adding two controlled switches between battery and SC, seven modes are identified based on the demanded power and SOC_{SC} . In the control strategy, different sets of control parameters are found for different driving cycles by using the searching method. For the new HESS system estimation, the battery degradation quantification shows 93.79%, 94.44%, and 82.72% of the theoretical mitigation potential of battery degradation on UDDS, HWFET and US06 are realized, respectively. Using an independent driving cycle as the test cycle, the simulation result shows the battery degradation mitigation reached as high as 30%, larger than the majority of the prior HESS. This result indicates that the HESS topology and control strategy can be optimized together to realize a better battery degradation mitigation target. When comparing the battery degradation with other HESS, the proposed HESS does not need the bi-directional converter, and achieves a competitive battery degradation mitigation result than the majority of the prior HESS. Furthermore, the temperature is a complicated factor that affects the HESS system. The temperature is a complicated factor. For a car with the same configuration, the vehicle's mileage is not constant across the different driving situations, including the temperature. We prefer to use the security factor to determine the size of the power system. In this paper, we only use the energy required to configure the battery and SC size. In our future research, the temperature factor will be considered in the HESS configuration.

Author Contributions: Total article structure design and writing, C.Z. and D.W.; Literature review and the funding support, B.W.; The battery degradation analysis and rearrange the paper structure, C.Z. and D.W.; The power calculation analysis and reviewed the paper before submitting, C.Z. and F.T. All authors have read and agreed to the published version of the manuscript.

Funding: This research received no external funding.

Conflicts of Interest: The authors declare no conflict of interest.

References

- Hannan, M.A.; Hoque, M.M.; Mohamed, A.; Ayob, A. Review of energy storage systems for electric vehicle applications: Issues and challenges. *Renew. Sustain. Energy Rev.* **2017**, *69*, 771–789. [[CrossRef](#)]
- Andwari, A.M.; Pesiridis, A.; Rajoo, S.; Martinez-Botas, R.; Esfahanian, V. A review of Battery Electric Vehicle technology and readiness levels. *Renew. Sustain. Energy Rev.* **2017**, *78*, 414–430. [[CrossRef](#)]
- Hoque, M.M.; Hannan, M.A.; Mohamed, A.; Ayob, A. Battery charge equalization controller in electric vehicle applications: A review. *Renew. Sustain. Energy Rev.* **2017**, *75*, 1363–1385. [[CrossRef](#)]
- Fathabadi, H. Novel fuel cell/battery/supercapacitor hybrid power source for fuel cell hybrid electric vehicles. *Energy* **2018**, *143*, 467–477. [[CrossRef](#)]
- Saxena, S.; MacDonald, J.; Moura, S. Charging ahead on the transition to electric vehicles with standard 120V wall outlets. *Appl. Energy* **2015**, *157*, 720–728. [[CrossRef](#)]
- Zhang, S.; Xiong, R.; Sun, F. Model predictive control for power management in a plug-in hybrid electric vehicle with a hybrid energy storage system. *Appl. Energy* **2017**, *185*, 1654–1662. [[CrossRef](#)]
- Wang, D.; Coignard, J.; Zeng, T.; Zhang, C.; Saxena, S. Quantifying electric vehicle battery degradation from driving vs. vehicle-to-grid services. *J. Power Sources* **2016**, *332*, 193–203. [[CrossRef](#)]
- Carkhuff, B.G.; Demirev, P.A.; Srinivasan, R. Impedance-Based Battery Management System for Safety Monitoring of Lithium-Ion Batteries. *IEEE Trans. Ind. Electron.* **2018**, *65*, 6497–6504. [[CrossRef](#)]
- Zhang, W.; Nie, J.; Li, F.; Wang, Z.L.; Sun, C. A durable and safe solid-state lithium battery with a hybrid electrolyte membrane. *Nano Energy* **2018**, *45*, 413–419. [[CrossRef](#)]
- Serhan, H.A.; Ahmed, E.M. Effect of the Different Charging Techniques on Battery Life-Time: Review. In Proceedings of the 2018 International Conference on Innovative Trends in Computer Engineering, ITCE, Aswan, Egypt, 19–21 February 2018; pp. 421–426. [[CrossRef](#)]
- Lipu, M.S.H.; Hannan, M.A.; Hussain, A.; Hoque, M.M.; Ker, P.J.; Saad, M.H.M.; Ayob, A. A review of state of health and remaining useful life estimation methods for lithium-ion battery in electric vehicles: Challenges and recommendations. *J. Clean. Prod.* **2018**, *205*, 115–133. [[CrossRef](#)]
- Ostadi, A.; Kazerani, M.; Chen, S.-K. Hybrid Energy Storage System (HESS) in vehicular applications: A review on interfacing battery and ultra-capacitor units. In Proceedings of the 2013 IEEE Transportation Electrification Conference and Expo (ITEC), Detroit, MI, USA, 16–19 June 2013; IEEE: Piscataway, NJ, USA, 2013; pp. 1–7. [[CrossRef](#)]
- Gallardo-Lozano, J.; Romero-Cadaval, E.; Milanés-Montero, M.I.; Guerrero-Martinez, M.A. Battery equalization active methods. *J. Power Sources* **2014**, *246*, 934–949. [[CrossRef](#)]
- Song, Z.; Li, J.; Han, X.; Xu, L.; Lu, L.; Ouyang, M.; Hofmann, H. Multi-objective optimization of a semi-active battery/supercapacitor energy storage system for electric vehicles. *Appl. Energy* **2014**, *135*, 212–224. [[CrossRef](#)]
- Shen, J.; Dusmez, S.; Khaligh, A. Optimization of Sizing and Battery Cycle Life in Battery/Ultracapacitor Hybrid Energy Storage Systems for Electric Vehicle Applications. *IEEE Trans. Ind. Inform.* **2014**, *10*, 2112–2121. [[CrossRef](#)]
- Ortuzar, M.; Moreno, J.; Dixon, J. Ultracapacitor-Based Auxiliary Energy System for an Electric Vehicle: Implementation and Evaluation. *IEEE Trans. Ind. Electron.* **2007**, *54*, 2147–2156. [[CrossRef](#)]
- Burke, A.F. Batteries and Ultracapacitors for Electric, Hybrid, and Fuel Cell Vehicles. *Proc. IEEE* **2007**, *95*, 806–820. [[CrossRef](#)]
- Kouchachvili, L.; Yaïci, W.; Entchev, E. Hybrid battery/supercapacitor energy storage system for the electric vehicles. *J. Power Sources* **2018**, *374*, 237–248. [[CrossRef](#)]
- Zhang, C.; Min, H.; Yu, Y.; Wang, D.; Luke, J.; Opila, D.; Saxena, S. Using CPE Function to Size Capacitor Storage for Electric Vehicles and Quantifying Battery Degradation during Different Driving Cycles. *Energies* **2016**, *9*, 903. [[CrossRef](#)]
- Cao, J.; Emadi, A. A New Battery/UltraCapacitor Hybrid Energy Storage System for Electric, Hybrid, and Plug-In Hybrid Electric Vehicles. *IEEE Trans. Power Electron.* **2012**, *27*, 122–132. [[CrossRef](#)]
- Blanes, J.M.; Gutiérrez, R.; Garrigós, A.; Lizán, J.L.; Cuadrado, J.M. Electric Vehicle Battery Life Extension Using Ultracapacitors and an FPGA Controlled Interleaved Buck–Boost Converter. *IEEE Trans. Power Electron.* **2013**, *28*, 5940–5948. [[CrossRef](#)]
- Odeim, F.; Roes, J.; Heinzl, A. Power Management Optimization of an Experimental Fuel Cell/Battery/Supercapacitor Hybrid System. *Energies* **2015**, *8*, 6302–6327. [[CrossRef](#)]

23. Song, Z.; Li, J.; Hou, J.; Hofmann, H.; Ouyang, M.; Du, J. The battery-supercapacitor hybrid energy storage system in electric vehicle applications: A case study. *Energy* **2018**, *154*, 433–441. [[CrossRef](#)]
24. Rizoug, N.; Mesbahi, T.; Sadoun, R.; Bartholomeüs, P.; Moigne, P.L. Development of new improved energy management strategies for electric vehicle battery/supercapacitor hybrid energy storage system. *Energy Effic.* **2018**, *11*, 823–843. [[CrossRef](#)]
25. Koubaa, R.; krichen, L. Double layer metaheuristic based energy management strategy for a Fuel Cell/Ultra-Capacitor hybrid electric vehicle. *Energy* **2017**, *133*, 1079–1093. [[CrossRef](#)]
26. Salmasi, F.R. Control Strategies for Hybrid Electric Vehicles: Evolution, Classification, Comparison, and Future Trends. *IEEE Trans. Veh. Technol.* **2007**, *56*, 2393–2404. [[CrossRef](#)]
27. Tani, A.; Camara, M.B.; Dakyo, B. Energy Management Based on Frequency Approach for Hybrid Electric Vehicle Applications: Fuel-Cell/Lithium-Battery and Ultracapacitors. *IEEE Trans. Veh. Technol.* **2012**, *61*, 3375–3386. [[CrossRef](#)]
28. Yuan, Z.; Teng, L.; Fengchun, S.; Peng, H. Comparative Study of Dynamic Programming and Pontryagin's Minimum Principle on Energy Management for a Parallel Hybrid Electric Vehicle. *Energies* **2013**, *6*, 2305–2318. [[CrossRef](#)]
29. Trovão, J.P.; Pereirinha, P.G.; Jorge, H.M.; Antunes, C.H. A multi-level energy management system for multi-source electric vehicles—An integrated rule-based meta-heuristic approach. *Appl. Energy* **2013**, *105*, 304–318. [[CrossRef](#)]
30. Naseri, F.; Farjah, E.; Ghanbari, T. An Efficient Regenerative Braking System Based on Battery/Supercapacitor for Electric, Hybrid, and Plug-In Hybrid Electric Vehicles with BLDC Motor. *IEEE Trans. Veh. Technol.* **2017**, *66*, 3724–3738. [[CrossRef](#)]
31. Wiczorek, M.; Lewandowski, M. A mathematical representation of an energy management strategy for hybrid energy storage system in electric vehicle and real time optimization using a genetic algorithm. *Appl. Energy* **2017**, *192*, 222–233. [[CrossRef](#)]
32. Santucci, A.; Sornioti, A.; Lekakou, C. Power split strategies for hybrid energy storage systems for vehicular applications. *J. Power Sources* **2014**, *258*, 395–407. [[CrossRef](#)]
33. Wang, L.; Collins, E.G.; Li, H. Optimal Design and Real-Time Control for Energy Management in Electric Vehicles. *IEEE Trans. Veh. Technol.* **2011**, *60*, 1419–1429. [[CrossRef](#)]
34. Battery Voltage Information—Battery University, BU-303: Confusion with Voltages. Available online: https://batteryuniversity.com/learn/article/confusion_with_voltages (accessed on 28 December 2019).
35. Smith, K.; Earleywine, M.; Wood, E.; Pesaran, A. Battery Wear from Disparate Duty-Cycles: Opportunities for Electric-Drive Vehicle Battery Health Management (Preprint). Available online: <https://www.nrel.gov/docs/fy13osti/54698.pdf> (accessed on 28 December 2019).
36. Wang, J.; Purewal, J.; Liu, P.; Hicks-Garner, J.; Soukazian, S.; Sherman, E.; Sorenson, A.; Vu, L.; Tataria, H.; Verbrugge, M.W. Degradation of lithium ion batteries employing graphite negatives and nickel-cobalt-manganese oxide + spinel manganese oxide positives: Part 1, aging mechanisms and life estimation. *J. Power Sources* **2014**, *269*, 937–948. [[CrossRef](#)]
37. IRGP4750DPBF Infineon Technologies Discrete Semiconductor Products DigiKey. Available online: <https://www.digikey.com/product-detail/en/infineon-technologies/IRGP4750DPBF/IRGP4750DPBF-ND/5149324> (accessed on 26 July 2018).
38. Hayes, J.G.; Davis, K. Simplified electric vehicle powertrain model for range and energy consumption based on EPA coast-down parameters and test validation by Argonne National Lab data on the Nissan Leaf. In Proceedings of the 2014 IEEE Transportation Electrification Conference and Expo (ITEC), Dearborn, MI, USA, 15–18 June 2014; IEEE: Piscataway, NJ, USA, 2014; pp. 1–6. [[CrossRef](#)]
39. DC-AC Sine Wave Inverters with High Input Voltage Deliver 100VA, ABSOPULSE Electron. Ltd. 2015. Available online: <https://absopulse.com/dc-ac-sine-wave-inverters-with-high-input-voltage-deliver-100va-csi-100-f2t-series/> (accessed on 26 July 2018).
40. Research Argonne National Laboratory. Available online: <http://www.anl.gov/energy-systems/research> (accessed on 26 July 2018).
41. Zhao, C.; Yin, H.; Ma, C. Quantitative Evaluation of LiFePO₄ Battery Cycle Life Improvement Using Ultracapacitors. *IEEE Trans. Power Electron.* **2016**, *31*, 3989–3993. [[CrossRef](#)]
42. Grbovic, P.J.; Delarue, P.; Moigne, P.L.; Bartholomeus, P. A Bidirectional Three-Level DC-DC Converter for the Ultracapacitor Applications. *IEEE Trans. Ind. Electron.* **2010**, *57*, 3415–3430. [[CrossRef](#)]

43. Sundaram, M.M.; Watcharatharapong, T.; Chakraborty, S.; Ahuja, R.; Duraisamy, S.; Rao, P.T.; Munichandraiah, N. Synthesis, and crystal and electronic structure of sodium metal phosphate for use as a hybrid capacitor in non-aqueous electrolyte. *Dalton Trans.* **2015**, *44*, 20108–20120. [[CrossRef](#)]
44. Rafik, F.; Gualous, H.; Gallay, R.; Crausaz, A.; Berthon, A. Frequency, thermal and voltage supercapacitor characterization and modeling. *J. Power Sources* **2007**, *165*, 928–934. [[CrossRef](#)]



© 2020 by the authors. Licensee MDPI, Basel, Switzerland. This article is an open access article distributed under the terms and conditions of the Creative Commons Attribution (CC BY) license (<http://creativecommons.org/licenses/by/4.0/>).